Journal of Catalysis **207,** 66–75 (2002)
doi:10.1006/jcat.2001.3489, available online at http://www.idealibrary.com on IDEAL®

Methane Reaction with NO over Alumina-Supported Ru Nanoparticles

Ioan Balint,*,[1] Akane Miyazaki,† and Ken-ichi Aika†

*Institute of Physical Chemistry, Romanian Academy, Spl. Independentei 202, 77208 Bucharest, Romania; and †Department of Environmental Chemistry and Engineering, Interdisciplinary Graduate School of Science and Technology, Tokyo Institute of Technology, 4259 Nagatsuta, Midori-ku, Yokohama 226-8502, Japan

Received October 1, 2001; revised December 3, 2001; accepted December 5, 2001

The reaction between NO (1%) and CH_4 (0.55%) over alumina supported Ru nanoparticles is analyzed from NO abatement, methane partial oxidation, and structural sensitivity points of view. The 6 and 12 wt% Ru/Al_2O_3 catalysts were prepared by deposition of well-defined colloidal Ru nanoparticles on alumina. The NO was selectively converted to N_2 starting from 450°C. Methane conversion to CO_x, H_2, and H_2O proved to be structure sensitive at 450°C and structure insensitive at $T > 450$°C. Methane was selectively converted to CO_2 at 450°C over the 12% Ru/Al_2O_3 catalyst having larger average Ru particle size (average particle size, 5.8 nm). Methane was oxidized to CO and CO_2 over the 6% Ru/Al_2O_3 catalyst with smaller Ru nanoparticles (average particle size, 4.8 nm). It is concluded that, at low temperature (450°C), methane is preferentially converted to CO and H_2 over small Ru nanoparticles. The highest reaction selectivity to CO (≈80%) and H_2 (≈78%) was observed at 600°C for both catalysts investigated. Ru/Al_2O_3 catalysts showed high and stable catalytic activity in time (i.e., 96 h), even at high reaction temperature (600°C). A selectivity to CO and H_2 of almost 100% was observed at 600°C for both a stoichiometric mixture of NO/CH_4 and one with an excess of methane. The catalyst with smaller Ru nanoparticles (6% Ru/Al_2O_3) was rapidly deactivated either by O_2 or by NO, whereas the catalyst with larger Ru particles (12% Ru/Al_2O_3) proved to be more resistant to oxygen poisoning. Both catalysts were rapidly reactivated in pure CH_4. A reaction mechanism is proposed in light of the experimental results.

Key Words: **Ru catalyst; methane partial oxidation; methane total oxidation; structure-sensitive reactions; NO selective reduction by methane.**

1. INTRODUCTION

The reaction of NO with CH_4 is a particularly interesting one and worthy of investigation from several points of view. From an environmental point of view it is clear that nitrogen oxides are extremely harmful pollutants and their removal is imperative. Methane reaction with NO can be also a subject of interest, especially if methane can be selectively oxidized to syngas (CO and H_2). The study of NO/CH_4 reaction from a structure sensitivity perspective is interesting as well because it provides deeper insight into the reaction mechanism.

To study together the aforementioned phenomena, a suitable catalytic system should be selected and prepared accordingly. The catalyst chosen in this study was Ru/Al_2O_3 because (i) ruthenium proved to be active and selective for the partial oxidation of methane (POM) (1), and (ii) well-structured metallic Ru nanoparticles can be obtained via the colloid method (2) (control of particle morphology is important in structure-sensitive reactions).

In this article the state of the art with respect to NO/CH_4 reaction is analyzed in more detail from environmental, POM, and structural sensitivity points of view.

The direct decomposition of NO, although thermodynamically favored, encounters serious difficulties because most of the catalysts are self-poisoned by the oxygen resulting from NO decomposition. Therefore, hydrocarbons (i.e., methane, ethylene, propylene) are used to remove the poisoning oxygen from the surface of the catalyst. Methane is one of them, which from economical point of view is very convenient because it is relatively inexpensive.

The oxidative conversion of methane to syngas is also favored from a thermodynamic point of view, but the problem lies in the deep oxidation of methane to CO_2 and water. Ru, Ni-based catalysts—perovskites, pyrochlores—have been reported to have a good activity and selectivity in POM reaction (3–6). The main problem is the high temperature required to achieve high conversion and selectivity (i.e., 850°C). The oxidizing agents typically used are oxygen and carbon dioxide (methane carbon dioxide reforming). To our knowledge, there are no published reports on POM using NO as oxidant.

Presumably, NO/CH_4 should be a structure sensitive reaction because it involves the formation of N–N bonds (7). It is well known that, in a structure-sensitive reaction, catalytic activity and selectivity are strongly related to the morphology of the supported metal particles (i.e., size and shape) (8). The conventional method of catalyst preparation, impregnation of the porous support (e.g., γ-Al_2O_3) with

[1] To whom correspondence should be addressed at the temporary address at the Tokyo Institute of Technology. Fax: +81-045-924-5441. E-mail: balint@chemenv.titech.ac.jp (or ibalint@chimfiz.icf.ro).

0021-9517/02 $35.00

an aqueous solution of a metal salt, yields structures consisting of metal particles that are nonuniform in size and shape and often too small to be characterized precisely. Additionally, the support has great influence on the activity of the metal when classic methods are used for catalyst preparation (9). We have shown in a series of articles that the catalytically active phase (metal) contains, depending on the impregnation conditions (temperature and pH) and the metal precursor used, variable amounts of aluminum as a result of support dissolution (10, 11).

It is somewhat surprising that information on the structural effects on the NO/CH_4 reaction is relatively scarce, although the reaction has been intensively investigated. In structure-sensitive reactions, morphological control of the supported metal particles is essential to obtain high catalytic activity and selectivity to the desired products (7). Therefore, a necessary step to a better understanding of the NO/CH_4 reaction mechanism is the preparation of catalysts with well-defined metal particles (size and/or crystal structure). A practical way to prepare well-defined metal particles is the colloid route. The major advantage of this method is that it provides relatively monodispersed metal particles. Additionally, the support effect on the active metallic phase is minimized because the metallic nanoparticles (i.e., Ru) are deposited onto the support after their formation is complete (2).

The aims of our research are (i) to support uniform colloidal Ru nanoparticles on alumina and then to test the specific catalytic activity for NO/CH_4 reaction; (ii) to gain insight into the reaction mechanism, and (iii) to prove a relationship exists between the structure of the supported Ru nanoparticles (size) and the catalytic activity as well as selectivity to specific reaction products.

2. EXPERIMENTAL

The Ru/Al_2O_3 catalyst was prepared by reduction of $RuCl_3$ with ethylene glycol in the presence of γ-alumina (Aerosil, 73 m^2 g^{-1}). The details of preparation are described elsewhere (2). Briefly, alumina was added under stirring to the ethylene glycol solution containing the dissolved $RuCl_3 \cdot 3H_2O$ (Wako Chemicals, purity >99%) to form a suspension. Then, the temperature of the suspension was slowly increased to 180°C to allow the reduction of $RuCl_3$ by the ethylene glycol on the surface of alumina. After ethylene glycol was removed by diluting the suspension with 0.3 M $NaNO_3$, the remaining solid was calcined at 500°C in air for 8 h to decompose the remaining organic phase (ethylene glycol). Two types of catalysts, containing 6 and 12% Ru on Al_2O_3, were prepared. The surface area of the final catalytic materials was similar to that of the initial support (alumina Aerosil).

The size distributions of the Ru nanoparticles supported on alumina for both catalysts were determined by TEM (Philips CM 20 transmission electron microscope). Additionally, the average size of the Ru nanoparticles was calculated by H_2 and CO chemisorption methods by assuming that each exposed Ru atom can adsorb one hydrogen atom or one CO molecule.

The concentration of Ru, both on the support and in the liquid phase after solid decantation, was determined by inductively coupled plasma (ICP) MS (Seiko SPS-4000) to evaluate the efficiency of Ru deposition on alumina.

X-Ray power diffraction analysis (Cu$K\alpha$ radiation) was carried out with a Rigaku Multiflex diffractometer provided with peak assignment software.

Temperature-programmed reduction (TPR) experiments were performed in a flow system with a quadrupole mass spectrometer (Anelva M-QA200TS) using a mixture of 5% H_2 in Ar and 0.05 g of catalyst. The heating rate and the total flow of the H_2–Ar mixture in TPR measurements were 10°C min^{-1} and 10 ml min^{-1}, respectively.

Activity tests of Ru/γ-Al_2O_3 catalysts for NO/CH_4 reaction were performed at atmospheric pressure with 0.05 g of catalyst loaded in a quartz microreactor (i.d. = 5 mm). The reactor was heated by a furnace connected to a temperature controller (Shimaden, Model SR 25). Electronic flow controllers (Kofloc, Model 3660) were used to control the flow of each reactant gas. The total flow rate of reactant mixture (NO in Ar and CH_4) was 50 cm^3 min^{-1} STP (standard temperature and pressure). The corresponding GHSV (gas hour space velocity) was 60,000 h^{-1}. The typical composition of the reactant mixture, using Ar as diluent, was 1% NO and 0.55% CH_4.

Effluent gases from the reactor were analyzed with a GL Sciences (Model 320) gas chromatograph equipped with TCD detectors. The typical reaction products were CO_x, N_2, and H_2O. H_2, N_2, NO, CH_4, and CO were separated and analyzed by using a molecular sieve 13X column, and CO_2 was analyzed using a Porapaq-Q column. Peak areas were measured using a Shimadzu (Model C-R 5A) electronic integrator.

The heating rate of the catalyst up to the reaction temperature was 10°C min^{-1}. At each temperature of investigation the catalyst was held at least 30 min in the reactant mixture to reach steady-state activity.

The activity of the catalyst is defined as the conversion [$X(\%)$] of the reactant (NO or CH_4) to all products,

$$X_{NO}(\%) = \frac{[NO]_{in} - [NO]_{out}}{[NO]_{in}} \times 100, \quad [1]$$

$$X_{CH_4}(\%) = \frac{[CH_4]_{in} - [CH_4]_{out}}{[CH_4]_{in}} \times 100, \quad [2]$$

where the subscripts "in" and "out" indicate the inlet and outlet concentrations of the reactant gases (NO and CH_4), respectively.

Reaction selectivity to CO [$S_{CO}(\%)$] and CO_2 [$S_{CO_2}(\%)$] is defined as

$$S_{CO}(\%) = \frac{[CO]}{[CO_2] + [CO]} \times 100, \quad [3]$$

$$S_{CO_2}(\%) = \frac{[CO_2]}{[CO_2] + [CO]} \times 100, \quad [4]$$

Reaction selectivity to H_2 (S_{H_2}) was deduced from the amount of CH_4 converted and from the resulting amount of H_2:

$$S_{H_2}(\%) = \frac{[H_2]}{\{[CH_4]_{in} - [CH_4]_{out}\} \times 2} \times 100. \quad [5]$$

3. RESULTS

The preparation variables, such as the concentration of Ru precursor in the organic phase (ethylene glycol) and reduction temperature, have great influence on the final morphology of the supported Ru nanoparticles. Generally, a high concentration of $RuCl_3$ in ethylene glycol and low reduction temperature favor the formation of large metal clusters followed by their aggregation. The optimal reduction temperature and concentration of $RuCl_3$ in ethylene glycol to obtain uniform Ru nanoparticles were found to be 180°C and 10^{-3} M, respectively.

Figure 1 presents comparatively the size distribution of the alumina-supported Ru nanoparticles for low (6% Ru/Al_2O_3) and high (12% Ru/Al_2O_3) metal loading as statistically determined from transmission electron micrographs.

The initial size distribution of the Ru nanoparticles for 6% Ru/Al_2O_3 is remarkably narrow, ranging between 3 and 6 nm. Around 78% of the Ru nanoparticles are either 4 or 5 nm. Larger (6 nm, around 21%) and smaller (3 nm, around 1%) Ru nanoparticles can be identified, as well. The average size of the Ru nanoparticles, determined statistically from transmission electron micrographs, was 4.8 nm.

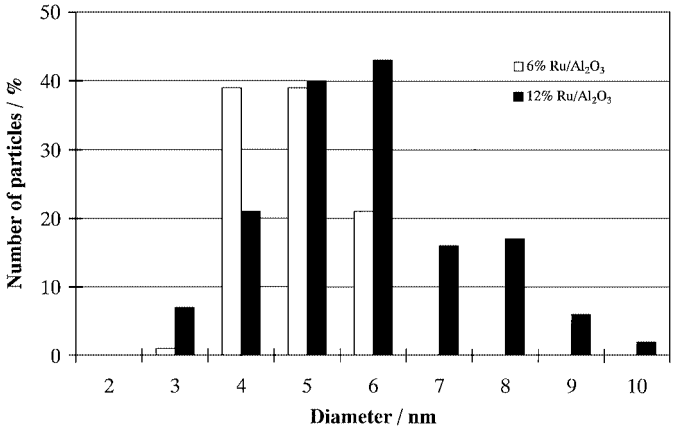

FIG. 1. Initial size distribution of the alumina supported Ru nanoparticles for 6% and 12% Ru/Al_2O_3 catalysts as determined from transmission electron micrographs.

TABLE 1

Average Size of Ru Nanoparticles, as Determined from Transmission Electron Micrographs and by H_2 and CO Chemisorption

Catalyst	Ru particle size (nm)		
	TEM	H_2	CO
6% Ru/Al_2O_2 (fresh)	4.8	4.8	5.4
6% Ru/Al_2O_2 (after more than 80 h time-on-stream in the temperature range 400–600°C)	7.6	—	—
12% Ru/Al_2O_3 (fresh)	5.8	5.7	5.9
12% Ru/Al_2O_3 (after more than 80 h time-on-stream in the temperature range 400–600°C)	8.9	—	—

In contrast to 6% Ru/Al_2O_3, the initial size distribution of the Ru nanoparticles for 12% Ru/Al_2O_3 is broader, ranging between 3 and 10 nm. Most of the Ru nanoparticles are 5 nm (≈26%) and 6 nm (≈28%) but there is also an important fraction of larger Ru particles ranging between 7 and 10 nm (≈26%). The average diameter of the Ru nanoparticles was 5.8 nm.

In addition to the TEM measurements, the average size of the alumina-supported Ru nanoparticles was determined by H_2 and CO adsorption (Table 1). It can be seen that there is a good agreement between the average size of Ru particles determined statistically from transmission electron micrographs and the average size estimated from chemisorption data.

Table 1 also shows that the supported Ru nanoparticles are subject to thermal coarsening with time. The average size of the alumina-supported Ru nanoparticles increased from 4.8 to 7.6 nm for 6% Ru/Al_2O_3 and from 5.8 to 8.9 nm for 12% Ru/Al_2O_3 after cycling up and down for more than 80 h in the temperature range 400–600°C.

3.1. Catalytic Activity for NO/CH_4 Reaction

The dependence of catalytic activity on reaction temperature for 6% Ru/Al_2O_3 is illustrated in Fig. 2. Conversion of NO at 400°C is close to zero (only traces of NO decomposed, for a short time, to N_2). An increase in temperature from 400 to 450°C led to a sudden increase in NO conversion, up to 100%. At any of the reaction temperatures, NO was selectively converted to N_2 over both Ru/Al_2O_3 catalysts investigated. On the other hand, methane was converted to CO_x, H_2, and H_2O. As expected, the amount of methane transformed tended to increase with increasing temperature. As can be seen in Fig. 2, the concentration of CO increased progressively with increasing temperature,

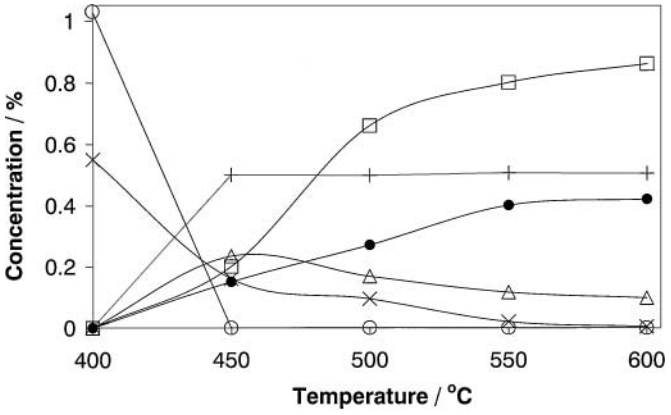

FIG. 2. NO reduction by CH_4 over 6% Ru/Al_2O_3 in the temperature range 400–600°C. (○) NO, (×) CH_4; (+) N_2; (△) CO_2; (●) CO; (□) H_2 (reaction mixture 1% NO, 0.55% CH_4, and balance Ar).

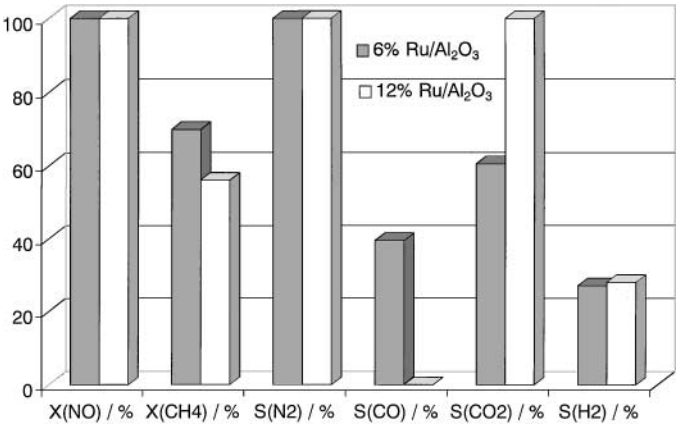

FIG. 4. Comparison between the catalytic behavior of 6 and 12% Ru/Al_2O_3 at 450°C for NO/CH_4 reaction (reactant mixture: 1% NO, 0.55% CH_4, and balance Ar).

from 0.16% at 450°C to 0.42% at 600°C. In contrast to CO, the concentration of CO_2 decreased with increasing reaction temperature, from 0.23% at 450°C to 0.1% at 600°C. The evolution of hydrogen closely follows that of CO. The concentration of H_2 increases with increasing reaction temperature from around 0.2% at 450°C to 0.86% at 600°C. As a consequence, water production (estimated from the chromatographic peak area) decreases as the reaction temperature is raised.

Similar to 6% Ru/Al_2O_3, the 12% Ru/Al_2O_3 catalyst exhibits a dependence on reaction temperature (Fig. 3). CO and H_2 production increased with increasing reaction temperature. The relatively poor carbon balance of ≈84% observed at 450°C is probably due to the support coking taking place in the first stage of reaction. However, the coking did not affect the activity of Ru/Al_2O_3 catalysts.

Comparisons between the catalytic behavior of 6% and 12% Ru/Al_2O_3 catalysts for NO/CH_4 reaction at the extreme temperatures of our study, 450 and 600°C, are presented in Figs. 4 and 5.

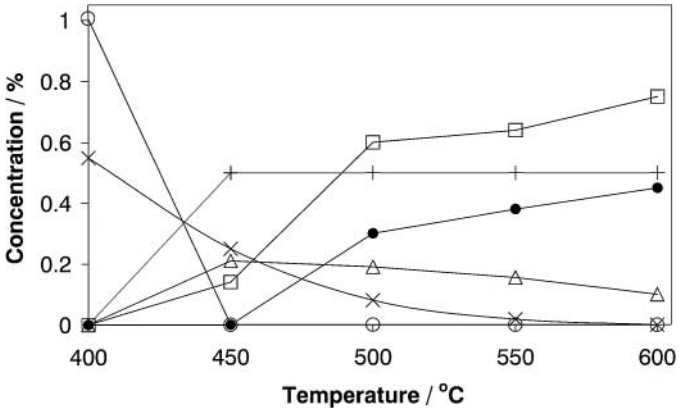

FIG. 3. NO reduction by CH_4 over 12% Ru/Al_2O_3 in the temperature range 400–600°C. (○) NO, (×) CH_4, (+) N_2, (△) CO_2, (●) CO, (□) H_2 (reaction mixture: 1% NO, 0.55% CH_4, and balance Ar).

At 450°C, the two catalytic materials investigated show significant differences in their activity and selectivity (Fig. 4). The catalyst (6%Ru/Al_2O_3) with smaller Ru nanoparticles has higher activity to methane conversion and higher selectivity to CO as compared with the catalyst (12% Ru/Al_2O_3) with larger Ru nanoparticles. Interestingly, at 450°C CH_4 is selectively converted to CO_2 and H_2O over 12% Ru/Al_2O_3 catalyst. This feature can be useful from the perspective of NO abatement since both CH_4 and NO are converted to nonharmful compounds, CO_2 and N_2, respectively.

Relatively similar catalytic behavior of the two catalysts investigated has been observed for $T > 450$°C. At 600°C, the conversion of NO and CH_4 is 100% and the selectivities to N_2, CO, and CO_2 for both catalysts are around 100, 80, and 20 respectively (Fig. 5). The only small difference is that the 6% Ru/Al_2O_3 catalyst has a slightly higher selectivity to H_2 (around 80%) as compared with the 12% Ru/Al_2O_3 catalyst (76%).

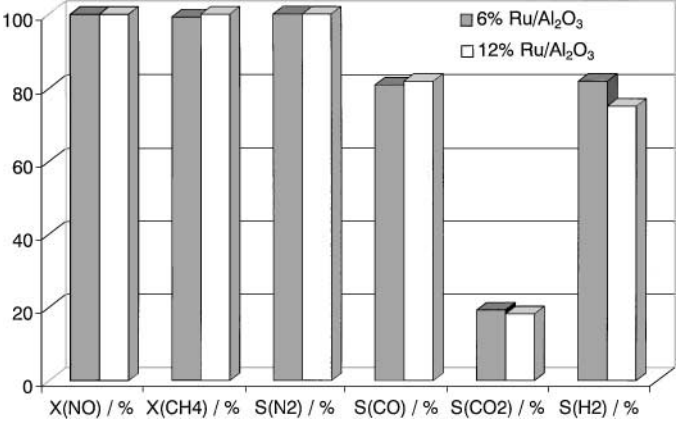

FIG. 5. Comparison between the catalytic behavior of 6 and 12% Ru/Al_2O_3 at 600°C for NO/CH_4 reaction (reactant mixture: 1% NO, 0.55% CH_4, and balance Ar).

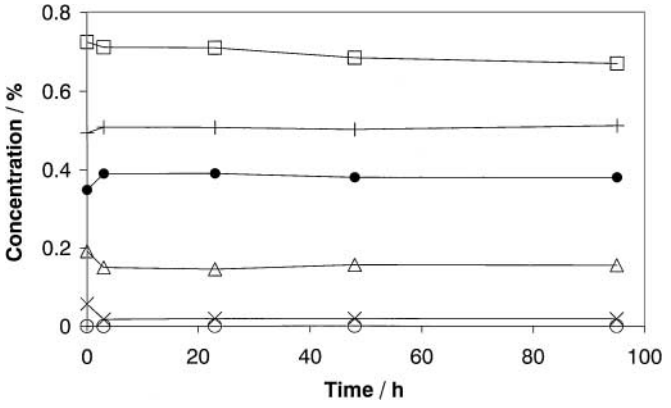

FIG. 6. Activity dependence on the time-on-stream at 550°C for 12% Ru/Al_2O_3 catalyst. (○) NO, (×) CH_4, (+) N_2, (△) CO_2, (●) CO, (□) H_2 (reaction mixture: 1% NO, 0.55% CH_4, and balance Ar).

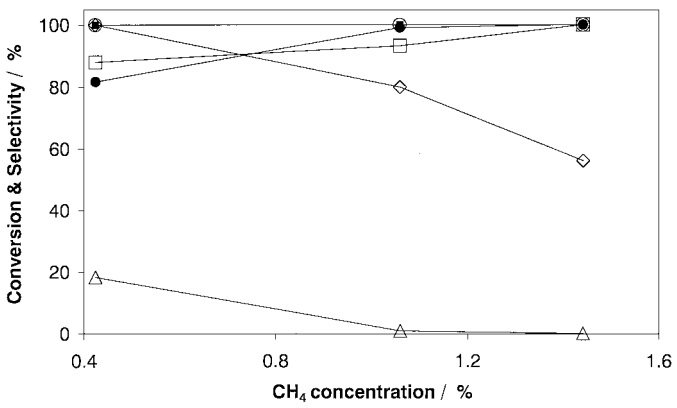

FIG. 7. Effect of CH_4 concentration on the 12% Ru/Al_2O_3 catalyst activity selectivity for NO/CH_4 reaction at 600°C. (○) NO conversion, (◇) CH_4 conversion, (■) selectivity to N_2, (△) selectivity to CO_2, (●) selectivity to CO, (□) selectivity to H_2 (the concentration of NO in reaction mixture was 0.8%).

It should be observed that the 6% Ru/Al_2O_3 catalyst is relatively sensitive to oxygen poisoning. In the absence of methane, the catalyst is rapidly deactivated either by air or by NO. The oxygen-deactivated catalyst can easily be reactivated by keeping it in pure methane for a few minutes at any of the reaction temperatures. On the other hand, the catalyst working in reaction mixture shows stable activity in time. Catalytic activity is not affected by carbon deposition (the catalyst shows approximately the same activity for NO/CH_4 reaction even after a long contact time with pure CH_4).

Both 6% Ru and 12% Ru/Al_2O_3 catalysts exhibit stable catalytic activity in time. Figure 6 illustrates, as an example, the catalytic activity of 12% Ru/Al_2O_3 at 550°C as a function of time-on-stream. Only a slight decrease in hydrogen production was observed for longer reaction time.

The NO/CH_4 reaction over 6% and 12% Ru/Al_2O_3 catalysts was performed under oxidation condition since the NO was in excess with respect to the stoichiometry of POM reaction. The concentration of CH_4 was increased to check if a stoichiometric mixture of oxidant (NO) and reductant can be selectively converted to syngas over Ru/Al_2O_3 catalyst. The reaction temperature selected was 600°C because at this temperature the selectivity to CO and H_2 for 12% Ru/Al_2O_3 catalyst is maximal (i.e., Fig. 3). From Fig. 7 it can be observed that at 600°C, reaction selectivity to CO and H_2 increases with increasing concentration of CH_4 in the reaction mixture. For a composition close to the stoichiometric one (0.8% NO–1.1% CH_4), reaction selectivities to CO and H_2 are 99 and 93%, respectively. For higher methane concentration, reaction selectivities to CO and H_2 are 100%.

3.2. Characterization of Ru/Al_2O_3 Catalysts by XRD and TPR

The 6% Ru/Al_2O_3 catalyst proved to deactivate rapidly under oxidation conditions, either in air (O_2) or in NO. XRD and TPR methods were used to elucidate the reasons for catalyst deactivation. XRD patterns of the deactivated (spectrum a) and active (spectrum b) 6% Ru/Al_2O_3 catalyst are comparatively presented in Fig. 8. It can be observed that for the active catalyst (spectrum b), the XRD reflections of metallic Ru are better resolved (better separation and higher peak intensity) as compared with those of deactivated catalyst (spectrum a). On the other hand, an increase in the intensity of the RuO_2 XRD peak at around $2\theta = 28°$ can be clearly observed for the deactivated catalyst. From this it can be concluded that (i) the catalytically active phase is related to metallic Ru state, and (ii) the RuO_2 form is inactive for NO/CH_4 reaction.

Figure 9 presents the TPR profiles of 6% Ru/Al_2O_3 catalysts, prepared by the deposition of Ru nanoparticles on alumina. Trace a represents the fresh catalyst, as it was after calcination at 500°C in air for 8 h. Trace b is the TPR profile of an active catalyst that worked for several hours in NO/CH_4 reaction mixture.

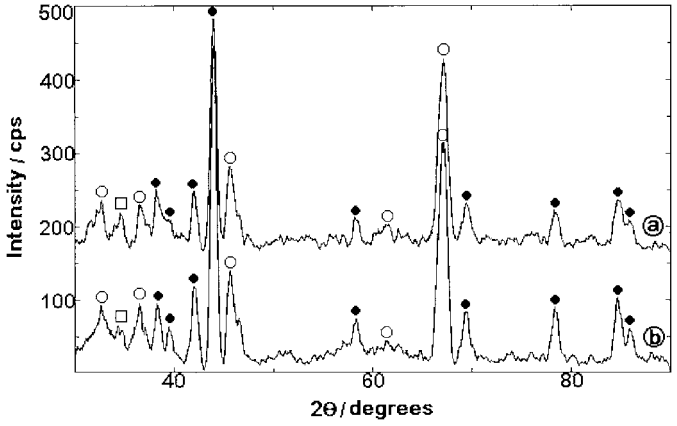

FIG. 8. XRD pattern of the 6% Ru/Al_2O_3 catalyst. (a) Catalyst deactivated by NO in the temperature range 400–600°C. (b) Active catalyst (working in NO/CH_4 reaction mixture). (●) Ru, (□) RuO_2, (○) Al_2O_3.

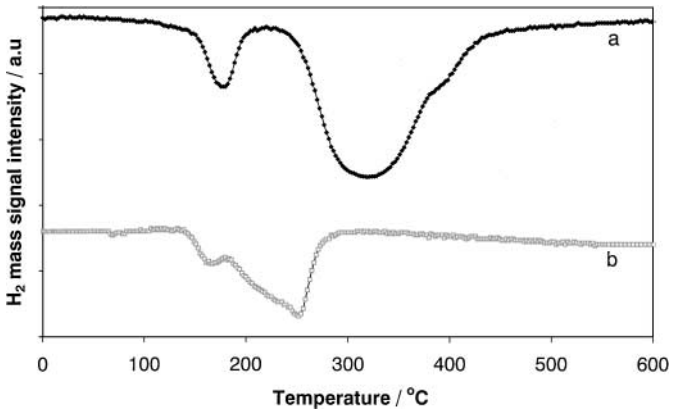

FIG. 9. TPR profiles of the 6% Ru/Al_2O_3 catalyst. (a) Catalyst prepared by Ru colloid deposition on alumina, calcined at 500°C in air for 8 h (fresh catalyst). (b) Catalyst working in reaction mixture (active catalyst) in the temperature range 400–600°C.

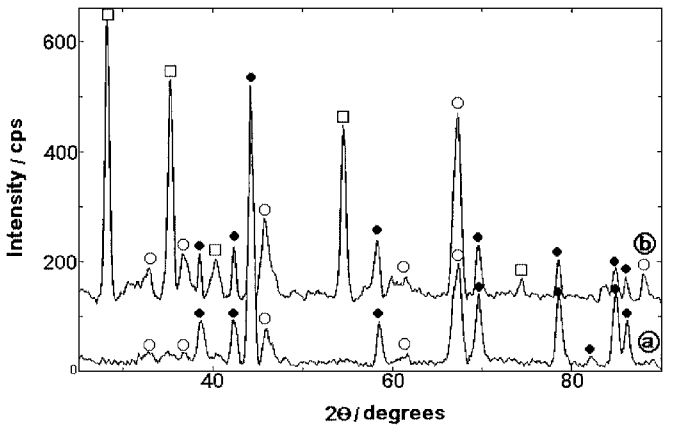

FIG. 10. XRD pattern of the 12% Ru/Al_2O_3 catalyst. (a) Active catalyst (working in the NO/CH_4 reaction mixture). (b) Catalyst partially deactivated after treatment with O_2 at 600°C for 1 h. (●) Ru, (□) RuO_2, (○) Al_2O_3.

Generally, the supported Ru catalyst exhibits two TPR peaks (12). The high-temperature peak is attributed to the reduction of RuO_2 that takes place, depending on the particle size, at $T > 220$°C. The fresh 6% Ru/Al_2O_3 catalyst (calcined at 500°C for 8 h) exhibits a large TPR peak 326°C and a smaller one at 182°C (trace a). It seems that some of the metallic Ru was oxidized to RuO_2 during the calcination process. Under reaction conditions (1% NO–0.55% CH_4), the amount of RuO_2 decreases as can be seen in Fig. 9, trace b. The high-temperature peak of the active 6% Ru/Al_2O_3, located at 254°C, is smaller than that of the calcined catalyst because the initial amount of RuO_2 decreased under reaction conditions. However, it is clear that the active 6% Ru/Al_2O_3 contains, besides the metallic Ru (main phase), small amounts of RuO_2 (see also Fig. 8, XRD pattern of the active catalyst).

The low-temperature TPR peaks of Fig. 9, located at around 170 and 182°C respectively, have been assigned to the reduction of well-dispersed RuO_x species (12). Looking at the size distribution presented in Fig. 1 and the TPR traces in Fig. 9, it becomes clear that the small Ru nanoparticles of the 6% Ru/Al_2O_3 catalyst were oxidized to RuO_x species during calcination in air or reaction.

The XRD and TPR results strongly suggest that the deactivation of 6% Ru/Al_2O_3 catalyst in an oxidizing atmosphere is due to the formation of RuO_x species, consisting mainly of RuO_2.

Figure 10 presents the XRD patterns of the active (spectrum a) and the partially deactivated (spectrum b) 12% Ru/Al_2O_3 catalyst. The catalyst was only partially deactivated during treatment with O_2 at 600°C for 1 h. The XRD spectrum of the active catalyst revealed only the reflections of metallic Ru (Fig. 10, spectrum a). The catalyst subjected to O_2 treatment partially lost its catalytic activity for NO/CH_4 reaction and the conversion of NO to N_2 at 600°C was only 80%. The only product of CH_4 oxidation on the partially deactivated catalyst was CO_2. It is likely that CO_2 formation took place via the reduction of RuO_2 by CH_4. The XRD pattern of the partially deactivated catalyst clearly demonstrates that the formation of RuO_2 is mainly responsible for catalyst deactivation (Fig. 10, spectrum b).

The fresh 12% Ru/Al_2O_3 catalyst calcined at 500°C for 8 h exhibits only the high-temperature TPR peak at 238°C (Fig. 11, trace a). Reduction of the RuO_2 species of 12% Ru/Al_2O_3 takes place more easily as compared with that of 6% Ru/Al_2O_3 since the high-temperature TPR peak of the former was detected at 326°C (Fig. 9, trace a). In contrast to 6% Ru/Al_2O_3, the calcined 12% Ru/Al_2O_3 catalyst shows a relatively high catalytic activity for NO/CH_4 reaction from the beginning. Prior to the catalytic reaction, the 6% Ru/Al_2O_3 required an activation procedure in reaction mixture (1% NO–0.55% CH_4) at 550°C to decrease the initial amount of RuO_2.

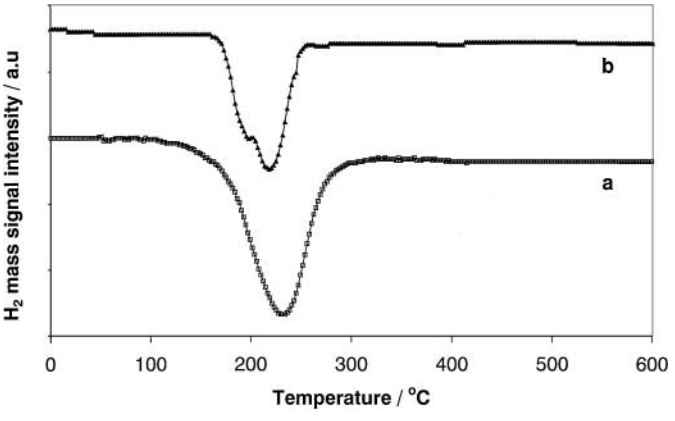

FIG. 11. TPR profiles of the 12% Ru/Al_2O_3 catalyst. (a) Catalyst calcined in air at 500°C for 8 h (fresh). (b) Catalyst (active form) after working for several hours in NO/CH_4 reaction mixture.

The TPR pattern of the working (active) 12% Ru/Al_2O_3 catalyst, presented in Fig. 11, trace b, exhibits both the high-temperature (223°C) and low-temperature (205°C) reduction peaks. From this it can be seen that even the active (working) catalyst contains some amount of RuO_2 and this gives the TPR peak at 223°C. The amount of RuO_2 in the active catalyst is smaller as compared with the calcined (fresh) one (Fig. 11, trace b). The XRD pattern of the working catalyst (active) did not evidence the presence of RuO_2 (Fig. 10) because the amount of RuO_2 was below the sensitivity of the XRD method.

From the results presented above it can be observed that the catalyst with larger Ru nanoparticles (12% Ru/Al_2O_3) better preserves its catalytic activity in an oxidizing atmosphere because the large Ru particles are more resistant to oxidation.

4. DISCUSSION

4.1. Dependence of the NO/CH_4 Reaction Stoichiometry on Temperature

Variation of the NO/CH_4 reaction stoichiometry with temperature, estimated from the activity tests, for 6 and 12% Ru/Al_2O_3 catalysts is presented in Table 2. Two regions can be distinguished. (i) In the low-temperature region (450°C) the low- and high-loading Ru catalysts behave distinctly. CH_4 is selectively oxidized to CO_2 over 12% Ru/Al_2O_3 catalyst, whereas over 6% Ru/Al_2O_3, methane is converted to both CO and CO_2. (ii) In the high-temperature region both catalysts exhibit relatively similar behavior.

The data presented in Table 2 show that the stoichiometry of NO/CH_4 reaction is strongly dependent on the reaction temperature. Production of CO and H_2 increases gradually, in parallel with the decrease in CO_2, with increasing reaction temperature. A tentative explanation for these results is given later.

TABLE 2

Variation of the NO/CH_4 Reaction Stoichiometry with Temperature for 6 and 12% Ru/Al_2O_3 Catalysts

Temp. (°C)	Catalyst	Reaction stoichiometry
450	6% Ru/Al_2O_3	$CH_4 + 3NO = 0.4CO + 0.6CO_2 + 0.6H_2 + 1.5N_2 + 1.4H_2O$
	12% Ru/Al_2O_3	$CH_4 + 3.5NO = CO_2 + 0.5H_2 + 1.75N_2 + 1.5H_2O$
500–600	6 and 12% Ru/Al_2O_3	$CH_4 + \underline{(1.6 \ldots 2.2)}NO = \underline{(0.6 \ldots 0.85)}CO + \underline{(0.4 \ldots 0.15)}CO_2 + \underline{(1.2 \ldots 1.6)}H_2 + \underline{(1.1 \ldots 0.8)}N_2 + \underline{(0.8 \ldots 0.4)}H_2O$

4.2. Considerations on the Formation of Primary Reaction Products

There is debate concerning the mechanism of formation of CO and H_2 in POM reaction. Some studies support the idea that CO_2 and H_2O are the primary reaction products of POM, whereas other studies point out that CO and H_2 are the initial reaction products. From isotope tracing experiments, performed in a closed system, it has been concluded that syngas production over Ru/Al_2O_3 catalysts takes place by total oxidation of methane followed by re-formation of the unconverted methane with carbon dioxide and steam to syngas (6). In fact, the specific feature of reactions performed in a closed system is the long contact time (duration of experiment) between the reaction products and reactants and the catalyst. Therefore, steam reforming of methane and carbon dioxide reactions, which are known to be slow processes, may have a significant impact on the final distribution of the reaction products. Under such experimental conditions (close system) the formation of H_2 as well as that of CO could not be observed because, if formed, these were readily oxidized to water and carbon dioxide, respectively, during the long contact time with the catalytic bed. In a FTIR study, Weng *et al.* (5) observed that on Ru/Al_2O_3 catalyst the formation of CO_2 proceeds much earlier than that of CO. The conclusion was that CO_2 is the primary reaction product of the O_2/CH_4 reaction. In reality, the above-presented results can be interpreted differently, if we take into consideration that the direct formation of CO and H_2 on the surface of the catalyst is a fast process. Direct formation of CO and H_2 sometimes is difficult to prove experimentally because these primary species are readily oxidized to CO_2 and H_2O, respectively. Indeed, there are studies that favor this hypothesis. Hickman and Schmidt (13) observed that for short contact time (0.01 s), the primary reaction products are H_2 and CO because the secondary reactions, such as methane steam reforming and water–gas shift reactions, are slow processes. The kinetic behavior of Ru/TiO_2 catalyst in the partial oxidation of methane indicates the direct formation of CO and H_2, while the reforming and water–gas shift reactions are negligible (14).

Thermodynamic calculations for partial oxidation of methane with oxygen differ significantly from our experimental data (1, 15). For example, at 600°C the theoretically predicted data for H_2/CO, CO_2/CO, and CH_4/CO ratios are 2.5, 1, and 0.25, respectively, whereas our experimental values for the same ratios are 1.7, 0.2, and 0 (see Figs. 2 and 3). The significant deviation of our data from thermodynamic equilibrium values suggests that, under our experimental conditions (short contact time, 0.06 s), the distribution of the reaction products is insignificantly affected by secondary equilibrium reactions (i.e., methane steam and carbon dioxide reforming, water–gas shift reaction) and therefore it is likely that both CO and H_2 are the primary reaction products. It is clear that the high selectivity to CO and H_2 at

low temperature indicates that the NO/CH_4 reaction over Ru/Al_2O_3 catalysts is occurring under nonequilibrium conditions.

4.3. Methane Conversion

4.3.1. Methane activation at low temperature (450°C). It is a general consensus that methane is activated on the catalytic surface during POM reaction by a homolytic splitting mechanism (3). For example, the POM reaction over Ni/Al_2O_3 was reported to take place via CH_4 pyrolysis (16). The major surface species are the adsorbed C or CH_x and H (13). After the surface reaction between C and oxygen, the resulting CO desorbs before further oxidation to CO_2 takes place. In the case of our supported Ru catalysts it is clear that, in the first stage of reaction, some of the initial RuO_2 is reduced and therefore the initial catalytic activity increases progressively with time to reach a steady state. TPR (Figs. 9 and 11) as well as XRD (Fig. 10) experiments revealed the presence of metallic Ru as well as a small amount of RuO_2 for the active ruthenium catalyst. The decrease in the initial amount of RuO_2 for the calcined (fresh) catalyst during the NO/CH_4 reaction in parallel with the increase in catalytic activity indicates that the catalytically active phase is metallic Ru.

Our experimental results strongly suggest that the key step in NO/CH_4 reaction is the homolytic splitting of CH_4 on the surface of Ru nanoparticles. High-resolution electron loss spectroscopy (HREELS) studies have shown that methane can dissociate easily on the surface of Ru, yielding methylidyne (CH), vinylidene (CCH_2), ethylidyne (CCH_3), and graphitic species (17). The degree of CH_4 dehydrogenation of Ru on the surface was observed to be dependent on temperature. Lower temperature favors the formation of CH_x species, whereas at higher temperatures ($T > 450$°C) only the graphitic phase is observed.

As we pointed out under Experimental, methane is selectively oxidized to CO_2 at 450°C over 12% Ru/Al_2O_3 catalyst, whereas over 6% Ru/Al_2O_3 catalyst, methane is converted to both CO and CO_2 (Fig. 4). It is clear that the mechanism of methane activation and CO_x formation is related to the size of Ru particles and to the reaction temperature. The formation of CO_2 at 450°C is favored over the catalyst (12% Ru/Al_2O_3) having larger Ru [$(Ru)_L$] particles.

On the other hand, the experimental results indicate that the formation of CO at low temperature (450°C) is related mainly to the small Ru particles ($d < 5$ nm). The formation of CO was observed only over 6% Ru/Al_2O_3 catalyst which has an important fraction of small Ru nanoparticles [(Ru_S)]. The larger Ru clusters of the same catalyst are likely to be responsible for the formation of CO_2.

In light of the results presented above it is rational to consider that methane dissociation at 450°C over Ru nanoparticles is dependent on the size of the Ru particles. The large Ru clusters ($d \geq 5$ nm) are less active at low temperature for methane dissociation and therefore methane splits into CH_x fragments ($0 \leq x \leq 3$) and hydrogen:

$$CH_4 + (Ru)_L \rightarrow (Ru)_L\text{–}CH_x + ((4 - x)/2)H_2. \quad [6]$$

The small Ru nanoparticles ($d < 5$ nm) should be more active for methane pyrolysis (17) and therefore methane is activated as C and H_2:

$$CH_4 + (Ru)_S \rightarrow C\text{–}(Ru)_S + 2H_2. \quad [7]$$

The next reaction step consists of the reaction between CH_x species and the O_{ads}, resulting from NO decomposition. On large Ru nanoparticles the formation of CO_2 takes place by the following reaction:

$$CH_x + ((4 + x)/2)O_{ads} \rightarrow CO_2 + (x/2)H_2O. \quad [8]$$

In reality, the reaction depicted by Eq. [8] should be the result of complex sequences of elementary reactions. The hydrogen from CH_x radicals may react with O_{ads} to give OH species, which then combine to form H_2O (13). However, the reactions involving CH_x and OH should almost inevitably lead to H_2O.

The interaction of NO (or oxygen) with metallic Ru cluster is also an important factor in NO/CH_4 reaction. We should remember that the 6% Ru/Al_2O_3 catalyst, with smaller Ru nanoparticles, is very sensitive to NO or O_2 poisoning. The explanation is that methane dissociates to CH_x species on a metallic Ru surface but not on the oxidized Ru surface (3). The 12% Ru/Al_2O_3 catalyst having larger Ru particles is less sensitive to oxygen poisoning because the larger the Ru particles are, the better the metallic character is preserved. Boudart (8) observed that the behavior of metal particles larger than 5 nm resembles that of bulk metal. Our TPR and XRD results (Figs. 8–11) prove that catalysts rich in RuO_x species (especially RuO_2) show little activity for POM reaction. The oxygen-deactivated catalyst can be easily reactivated by keeping it in pure CH_4 for a few minutes. In conclusion, larger Ru clusters are more suitable for NO/CH_4 reaction because they are more resistant to oxygen poisoning.

The carbon formed on small Ru particles is selectively oxidized to CO by the O_{ads} resulting from NO:

$$C\text{–}(Ru)_S + O_{ads} \rightarrow (Ru)_S + CO. \quad [9]$$

Oxidation of the superficial carbon species selectively gives CO, because the graphitic species shows relatively low chemical reactivity (17).

In conclusion, the structural effects observed at 450°C are related to the way in which methane is activated over Ru nanoparticles. Larger Ru nanoparticles activate methane as CH_x and hydrogen, whereas small Ru nanoparticles (more active) activate methane as carbon and hydrogen. The

surface oxidation of CH_x species gives carbon dioxide and water, whereas the oxidation of bare carbon selectively gives CO.

As we will see, above 450°C the size of the metal particles is not an important parameter anymore, and therefore the NO/CH_4 reaction becomes structure insensitive. The activity and selectivity to reaction products are relatively the same for both catalysts investigated.

4.3.2. Methane activation in the temperature range 500–600°C. An increase in temperature ($T > 450$°C) leads to an increase in CO production at the expense of CO_2 for both catalysts (selectivity to CO increases with increasing temperature) (Figs. 2–5). Moreover, the evolution of CO, CO_2, and H_2 with temperature is similar for both catalysts. In the high-temperature domain, the size of the Ru particles has no influence on the reaction selectivity to CO, CO_2, and H_2. Experimental results suggest that the formation of water is connected to the activation of methane as CH_x species. In other words, the presence of hydrogen (as CH_x) on the surface of the metal leads to the formation of water via reaction between CH_x and O_{ads}. If we assume that for $T > 450$°C methane decomposition over large Ru clusters gives CH_x, and over small Ru clusters gives C, the simultaneous formation of CO (by the oxidation of C) and CO_2 and H_2O (by the oxidation of CH_x) can be well explained. It is rational to consider that the increase in CO and H_2 production with increasing reaction temperature is due to the increase in activity of the large Ru clusters for methane decomposition with increasing temperature. The ratio of hydrogen to carbon in CH_x radicals decreases (the x coefficient of hydrogen decreases) with increasing temperature and therefore the formation of CO_2 and H_2O is drastically reduced. At 600°C, selectivity to CO and to H_2 is around 80% for both catalysts (Fig. 5).

It is probable that the decomposition of CH_4 on the surface of Ru nanoparticles is an equilibrium process. If the concentration of methane in the reaction mixture is increased, the decomposition equilibrium is shifted to the formation of carbon and hydrogen ($CH_4 \leftrightarrow CH_x + H_2 \leftrightarrow C + H_2$). Experimental results confirm this assumption. When the concentration of CH_4 was increased from 0.5 to ≈1%, reaction selectivity to CO and H_2 at 600°C was close to 100% and formation of water was not observed.

In summary a simplified mechanism of NO/CH_4 reaction over alumina-supported Ru catalyst is proposed in Fig. 12.

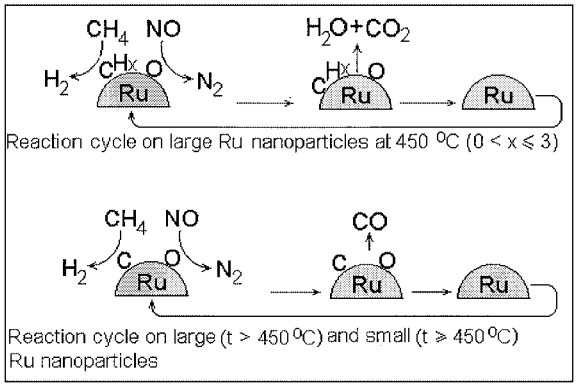

FIG. 12. Simplified model describing the mechanism of NO/CH_4 reaction over Ru nanoparticles supported on alumina.

4.4. NO Activation

NO decomposes easily after adsorption, to give N_{ads} and O_{ads} on the surface of reduced metals (18). The decomposition of NO leaves O_{ads} on the surface of metal and this blocks the active sites for further NO decomposition (19). The reaction is self-poisoned by oxygen. Therefore, a reductant should be used to regenerate the metal active sites (to create surface vacant places for further decomposition of NO). It was suggested that the relative activities of the various catalysts reflect the ease of reduction of catalyst by a reducing agent (20, 21).

It is believed that the reduction of NO by hydrocarbons takes place by a two-step mechanism (22). The reaction is initiated by one molecule of hydrocarbon reducing a small part of the Me–O surface into a metallic surface (i.e., Pt, Pd, Rh). Once a vacancy is created a surface explosion occurs. Experimental results show that the conversion of NO increases suddenly from zero to 100% in a narrow temperature range (400–450°C) (Figs. 2 and 3).

NO is selectively converted to N_2 over both Ru catalysts investigated. Formation of N_2O or NH_3 was not observed at any of the reaction temperatures. In contrast to the Ru catalyst, the supported precious metals (Pt, Pd, and Rh) give high selectivity to N_2O in a lower temperature range or to NH_3 in a higher temperature range (21, 22).

Burch *et al.* (20–22) advanced the idea that, on precious metals, N_2O is formed by the reaction between NO_{ads} and N_{ads}, and NH_3 is formed by the reaction between $(CH_x)_{ads}$ and N_{ads}. The absence of N_2O for supported ruthenium catalysts can be attributed to the complete dissociation of the adsorbed NO, because if there was any molecularly adsorbed NO on the surface of Ru nanoparticles, N_2O could be produced by the reaction between NO_{ads} and N_{ads}. Probably N_{ads} desorbs rapidly as N_2 after the decomposition of NO. This also explains the absence of NH_3 in the reaction products for supported Ru catalysts.

5. CONCLUSIONS

1. NO is selectively reduced by CH_4 to N_2 over well-defined Ru nanoparticles supported on γ-Al_2O_3 starting from 450°C.

2. At 450°C, CH_4 is selectively oxidized by NO to CO_2 and H_2O over the catalyst (12% Ru/Al_2O_3) with larger Ru nanoparticles ($d \geq 5$ nm).

3. CH_4 is directly converted by NO to CO and H_2 over small Ru nanoparticles ($d < 5$ nm) in the temperature range 450–600°C.

4. The catalyst with a larger fraction of small Ru nanoparticles (6% Ru/Al_2O_3) is easily deactivated either by air or by NO, whereas the catalyst with larger Ru nanoparticles (12% Ru/Al_2O_3) is less sensitive to oxygen poisoning.

5. The key point of the reaction mechanism is CH_4 activation over Ru nanoparticles. (i) At 450°C, CH_4 molecules split into CH_x fragments and H_2 ($0 < x \leq 3$) over large Ru naparticles. CH_x species are further selectively oxidized by O_{ads} to CO_2 and H_2O. (ii) CH_4 splits into C and H_2 over small Ru particles. The C is further oxidized by O_{ads} to CO.

ACKNOWLEDGMENT

A research grant from the Japanese Society for the Promotion of Science (No. P00136) is greatly appreciated.

REFERENCES

1. Tsang, S. C., Claridge, J. B., and Green, M. L. H., *Catal. Today* **23**, 3 (1995).
2. Miyazaki, A., Balint, I., Aika, K., and Nakano, Y., *J. Catal.* **204**, 364 (2001).
3. Peña, M. A., Gomez, J. P., and Fierro, J. L. G., *Appl. Catal. A* **144**, 7 (1996).
4. Roh, H.-S., Jun, K.-W., Dong, W.-S., Park, S.-E., and Joe, Y.-I., *Chem. Lett.* 666 (2001).
5. Weng, W. Z., Chen, M. S., Yan, Q. G., Wu, T. H., Chao, Z. S., Liao, Y. Y., and Wan, H. L., *Catal. Today* **63**, 317 (2000).
6. Guerrero-Ruiz, A., Ferreira-Apparicio, P., Bachiller-Baeza, M. B., and Rodriguez-Ramos, I., *Catal. Today* **46**, 99 (1998).
7. Gates, B. C., *Chem. Rev.* **95**, 511 (1995).
8. Boudart, M., *J. Mol. Catal.* **30**, 27 (1985).
9. Hayek, K., Kramer, R., and Paál, Z., *Appl. Catal. A* **162**, 1 (1997).
10. Balint, I., Miyazaki, A., and Aika, K., *Chem. Mater.* **11**, 378 (1999).
11. Balint, I., Miyazaki, A., and Aika, K., *Chem. Mater.* **13**, 932 (2001).
12. Betancourt, P., Rives, A., Hubaut, R., Scott, C. E., and Goldwasser J., *Appl. Catal. A* **170**, 307 (1998).
13. Hickman, D. A., and Schmidt, L. D., *J. Catal.* **138**, 267 (1992).
14. Elmasides C., Ioannides T., and Verykios X. E., *AIChE J.* **46**, 1260 (2000).
15. Zhu, J., Zhang, D., and King, K. D., *Fuel* **80**, 899 (2001).
16. Lu, Y., Xue, J., Yu, C., Liu, Y., and Shen, S., *Appl. Catal. A* **174**, 121 (1998).
17. Choudhary, T. V., and Goodman, D. W., *J. Mol. Catal.* **163**, 9 (2000).
18. Comrie, C. M., Weinberg, W. H., and Lambert, R. M., *Surf. Sci.* **57**, 619 (1976).
19. Walker, A. V., Gruyters, M., and King, D. A., *Surf. Chem.* **384**, L791 (1997).
20. Burch, R., and Ramli, A., *Appl. Catal. B* **15**, 49 (1998).
21. Burch, R., and Ramli, A., *Appl. Catal. B* **15**, 63 (1998).
22. Burch, R., and Millington, P. J., *Catal. Today* **26**, 185 (1995).